View metadata, citation and similar papers at core.ac.uk

brought to you by CORE

provided by Kyutacar : Kyushu Institute of Technology Academic Repository

九州工業大学学術機関リポジトリ
Kyutacar
Kyushu Institute of Technology Academic Repository

Anomalous spiked structures in ESR signals from the chiral helimagnet CrNb3S6

著者	Yoshizawa Daichi, Sawada Yuya, Kousaka Yusuke, Kishine Jun-ichiro, Togawa Yoshihiko, Mito Masaki, Inoue Katsuya, Akimitsu Jun, Nakano Takehito, Nozue Yasuo, Hagiwara Masayuki
journal or publication title	Physical review B
volume	100
number	10
page range	104413-1-104413-6
year	2019-09-09
URL	http://hdl.handle.net/10228/00007988

doi: https://doi.org/10.1103/PhysRevB.100.104413

Anomalous spiked structures in ESR signals from the chiral helimagnet $CrNb_3S_6$

Daichi Yoshizawa,[1] Yuya Sawada,[1] Yusuke Kousaka,[2,3] Jun-ichiro Kishine,[3,4] Yoshihiko Togawa,[3,5] Masaki Mito,[3,6] Katsuya Inoue,[3,7] Jun Akimitsu,[2,3] Takehito Nakano,[8] Yasuo Nozue,[8] and Masayuki Hagiwara[1,3,*]

[1]*Center for Advanced High Magnetic Field Science, Graduate School of Science, Osaka University, Toyonaka, Osaka 560-0043, Japan*
[2]*Research Institute for Interdisciplinary Science, Okayama University, Okayama, Okayama 700-8530, Japan*
[3]*Center for Chiral Science, Hiroshima University, Higashihiroshima, Hiroshima 739-8526, Japan*
[4]*Division of Natural and Environmental Science, The Open University of Japan, Mihama, Chiba 261-8586, Japan*
[5]*Department of Physics and Electronics, Osaka Prefecture University, Sakai, Osaka 599-8531, Japan*
[6]*Faculty of Engineering, Kyusyu Institute of Technology, Kitakyushu, Fukuoka 804-8550, Japan*
[7]*Graduate School of Science, Hiroshima University, Higashihiroshima, Hiroshima 739-8526, Japan*
[8]*Department of Physics, Graduate School of Science, Osaka University, Toyonaka, Osaka 560-0043, Japan*

(Received 7 March 2018; revised manuscript received 17 April 2019; published 9 September 2019)

We have performed X-band electron spin resonance (ESR) measurements on a single crystal of the metallic chiral helimagnet $CrNb_3S_6$ from 3.5 to 180 K and for the external magnetic fields H_{ext}, up to 4 kOe, perpendicular to the c axis (the helical axis of $CrNb_3S_6$). This field-crystalline configuration is expected to provide the chiral soliton lattice (CSL) state in this system. The main resonance line can be fit with a Dysonian function above $T_c = 127$ K, but additional features in the spectra were observed below 105 K. Specifically, spiked anomalies superposed on the main signals were observed for magnetic fields between H_{c1} and H_{c2} that are the appearing and disappearing fields of the spiked anomalies, respectively. The resulting magnetic field vs temperature phase diagram possesses three regions, which are interpreted as different dynamical responses in the CSL phase. In addition, the values of H_{c2} are close to those reported by the d^2M/dH^2 curve [Tsuruta *et al.*, Phys. Rev. B **93**, 104402 (2016)]. Furthermore, the field range between H_{c1} and H_{c2}, where the spiked anomalies exist, depends on the field direction and shifts to higher fields when turning to the c axis, thereby providing additional evidence that these spiked anomalies must be related to the chiral soliton dynamics.

DOI: 10.1103/PhysRevB.100.104413

I. INTRODUCTION

Chirality, left-handedness or right-handedness in symmetrical properties, plays a crucial role in nature. Some compounds with crystallographic chirality are named as chiral helimagnets (CHMs). The uniform Dzyaloshinskii-Moriya (DM) interaction, an antisymmetric interaction induced by the absence of inversion symmetry between neighboring magnetic ions [1–3], and the exchange interaction cause the chiral helical magnetic structure below a long-range ordering temperature. In order to show how to construct the chiral helical magnetic structure, we simply consider a one-dimensional (1D) CHM given by the following Hamiltonian:

$$\mathcal{H} = -J\sum_i \boldsymbol{S}_i \cdot \boldsymbol{S}_{i+1} - \sum_i \boldsymbol{D} \cdot (\boldsymbol{S}_i \times \boldsymbol{S}_{i+1}) - g\mu_B \sum_i \boldsymbol{H} \cdot \boldsymbol{S}_i. \tag{1}$$

Here, the first, second, and third terms represent the ferromagnetic (FM) exchange interaction ($J > 0$) between the nearest-neighbor (NN) spins, the uniform DM interaction between the NN spins, and the Zeeman interaction, respectively. The uniform DM interaction gives twists in the 1D FM chain, so the competition between the FM and the DM effects create the chiral helical magnetic state. This state has already been observed in several chiral materials, for example, MnSi [4], $Fe_{1-x}Co_xSi$ [5], and $CrNb_3S_6$ [6].

In the presence of an external magnetic field H_{ext}, peculiar magnetic states emerge in these CHMs, and the skyrmion lattice is one notable example. In this state, the magnetic vortices, i.e., skyrmions, form a triangular lattice, which has been observed in small angle neutron scattering and Lorentz transmission electron microscopy measurements [7–9]. A different peculiar state appears in magnetic fields perpendicular to the helical axis of the CHMs. Under these conditions, the helical structure is unwound periodically, resulting in a magnetic structure constructed by alternate FM and helical structures. This arrangement is known by several names, including helicoid, magnetic kink crystal, and chiral soliton lattice (CSL), which is the terminology that will be used hereafter. In this CSL state, the FM region widens with increasing magnetic field, and finally, all of the magnetic moments point along the field direction above the saturation magnetic field H_{sat}. This CSL state was first theoretically proposed by Dzyaloshinskii [10], and its characteristic features have been theoretically investigated in recent years [11–13], and some of them were experimentally observed [14–19].

$CrNb_3S_6$ is one of the materials in which the CSL state appears. Magnetic Cr^{3+} ions are intercalated in the $2H$-type NbS_2 layers, and these Cr^{3+} ions construct the two-dimensional layers. The centrosymmetry is broken due to the

*Corresponding author: hagiwara@ahmf.sci.osaka-u.ac.jp

 ©2019 American Physical Society

intercalation of the Cr^{3+} ions, and then, $CrNb_3S_6$ belongs to the noncentrosymmetric hexagonal space group $P6_322$, which allows the uniform DM vector along the c axis [6,20–22]. The lattice constants at room temperature are $a = 5.75$ Å and $c = 12.12$ Å [6,20,22]. The chiral helical magnetic structure with a long period along the c axis below the long-range ordering temperature T_c (=127 K in our sample) was observed by the neutron scattering [6] and electron beam [14] measurements. The magnetic helical pitch is 480 Å (48 nm), corresponding to about 40 unit cells, in the lower temperature region. For the $H_{ext} \perp c$ axis, the CSL state emerges below H_{sat}~2000 Oe. Our previous electron spin resonance (ESR) [23] study with the $H_{ext} \| c$ axis and a theoretical study to explain some experimental resutls of $CrNb_3S_6$ [24] indicated that both the inter- and intralayer interactions are ferromagnetic and that the intralayer interactions are about ten times larger than the interlayer ones. Thus, the magnetic structure of this compound is explained as two-dimensional (2D) FM layers which align along the c axis with twisting as depicted in Fig. 1 of Ref. [13]. With the $H_{ext} \perp c$ axis, the period of the CSL state was observed to increase gradually up to about H_{sat}. In the vicinity of H_{sat}, a dramatic increase of the period was detected [14], and this change is also evidenced in magnetization measurements [18,25]. These unusual features of the static magnetic response of the CSL state for the $H_{ext} \perp c$ axis motivated the present study of the dynamical behavior [26,27].

In this study, we have performed X-band ($f = 9.28$ GHz) ESR measurements of a single crystal of $CrNb_3S_6$. We observed a signal with the shape of the Dysonian function above 130 K, a deformed signal between 110 and 130 K, and then spiked anomalies, which appear and disappear at certain fields defined as H_{c1} and H_{c2}, superposed on some unusual ESR signals below 110 K. We discuss the features of the ESR signals and the field region of the spiked anomalies by comparing with the ac magnetization results [25] in the magnetic field versus temperature (H-T) phase diagram.

II. EXPERIMENT

Single-crystal samples of $CrNb_3S_6$ were synthesized by a chemical transport method, and the details of the synthesis are described in Ref. [21]. The size of our samples is about $1 \times 1 \times 0.1$ mm^3 (the c axis is along the shortest-size direction) and thus our sample is regarded as a bulk crystal. The qualities of the samples were checked by the x-ray diffraction measurements, and no impurity phase was found in the samples.

The temperature dependence of ESR signals were measured with an X-band ESR apparatus (Bruker EMX ESR spectrometer). The sample was mounted on a quartz rod by vacuum grease and the rod was inserted into the resonant cavity. The external magnetic field H_{ext} and the microwave oscillating magnetic field H_{mw} were applied perpendicular to the c axis. The field derivative of ESR absorption curve was obtained by the field modulation technique while data were acquired during isothermal field sweeps at temperatures in the range 3.5–180 K.

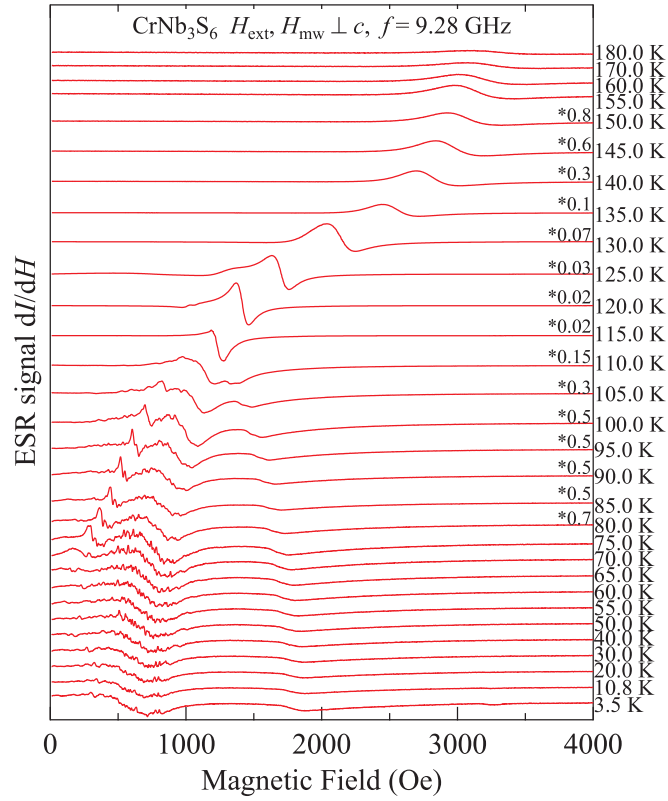

FIG. 1. Temperature dependence of ESR signals of a single crystal of $CrNb_3S_6$ at 9.28 GHz for $H_{ext} \perp c$ and $H_{mw} \perp c$. The asterisked numbers on the right side of the plot indicate the scaling factors used to reduce the size of the ESR signals in the plot.

The magnetization of the single crystal of $CrNb_3S_6$ was measured by using a superconducting quantum interference device magnetometer (Quantum Design MPMS-XL7).

III. RESULTS AND ANALYSES

Figure 1 shows the temperature dependence of the ESR signals of a single crystal of $CrNb_3S_6$ at the measurement frequency $f = 9.28$ GHz for $H_{ext} \perp c$ and $H_{mw} \perp c$. For 130 K $< T <$ 180 K, we observe an ESR signal that gradually shifts to lower fields with decreasing temperature down to 145 K and then drastically shifts below 140 K. The signal in this temperature range can be fitted by a single Dysonian function. Below 125 K, which is close to the transition temperature $T_c = 127$ K, the shape of the signal starts to deform, and the signal splits into several lines. In addition, the signal intensity becomes large near this temperature, and the data have been scaled by a factor given in the figure. Eventually at lower temperqatures, the lowest-field signal shifts to the low field side and is not observed below 65 K, and the shapes of the other signals are almost unchanged below 90 K. The spiked anomalies, which look like noise on the baseline, start to appear near 1000 Oe at 105 K. The field range and the characteristics of these spiked anomalies will be described later in Sec. IV. This unusual phenomenon emerges in the presence of the field below H_{sat}, and hence it must be related to the CSL state. In the following sections, we will discuss the features of the aforementioned ESR signals separately above and below T_c.

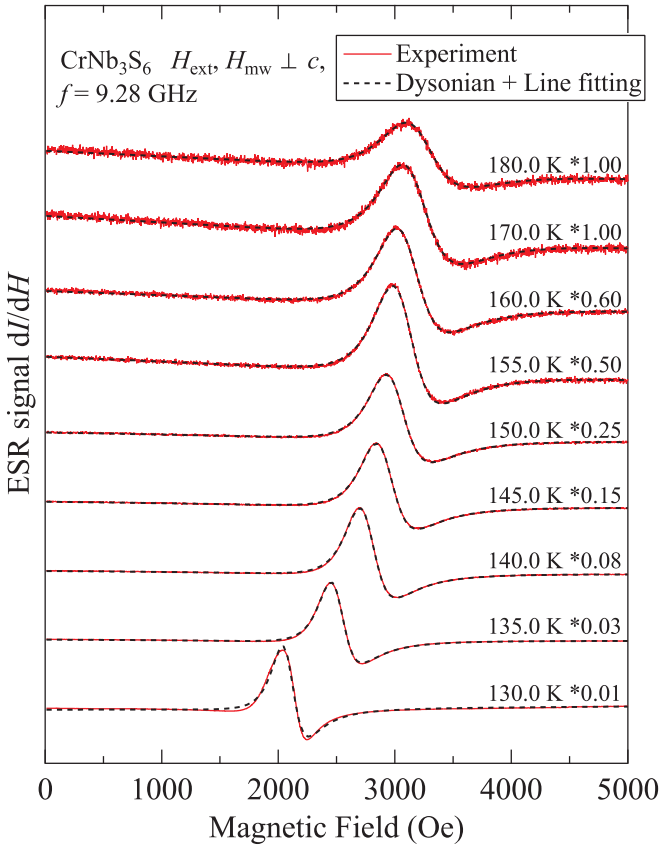

FIG. 2. ESR signals of a single crystal of $CrNb_3S_6$ together with the fitting results by a single Dysonian function above T_c. The red solid and black broken lines indicate the experimental and the fitting results, respectively. The numbers with an asterisk next to the temperatures have the same meanings as in Fig. 1.

A. Above the transition temperature ($T > T_c$)

We can fit the spectra above T_c by using a single Dysonian function,

$$f_{\text{Dysonian}}(H) = I_D \frac{d}{dH}\left(\frac{W_D + \alpha(H - H_{\text{res}})}{(H - H_{\text{res}})^2 + W_D^2}\right), \qquad (2)$$

where I_D, W_D, H_{res}, and α in Eq. (2) are the signal intensity, the half width at half maximum, the resonance field, and the dispersion to absorption ratio of the signal, respectively [28,29]. The Dysonian function, Eq. (2), represents the ESR absorption in a metallic sample. Here, the dispersion to absorption ratio $0 < \alpha \leqslant 1$ is related to metallic properties of the sample, for example, sample size, geometry, and skin depth. If the skin depth is small compared to the sample size, then $\alpha \to 1$. On the other hand, when the sample is an insulator, $\alpha \to 0$, and then Eq. (2) changes into the Lorentzian function. Figure 2 shows the results of fitting the ESR signals with Eq. (2) at several temperatures above T_c.

In Fig. 3, all the ESR signals, with the exception of the data at 130 K, are fitted with $\alpha \sim 1$, suggesting the Cr^{3+} spins exist in a good metallic environment. Usually, the ESR signal intensities are proportional to the magnetization values in the paramagnetic state. Therefore, we compare the ESR signal intensities with the magnetizations of $CrNb_3S_6$ at the

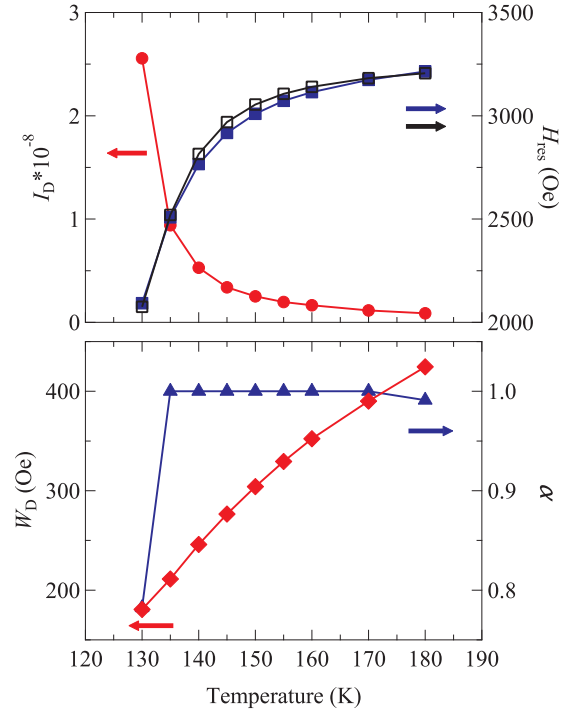

FIG. 3. Fitting parameters I_D, H_{res}, W_D, and α [Eq. (2)] for the ESR signals of $CrNb_3S_6$ as a function of temperature. The open black squares with a line indicate the calculated ferromagnetic resonance fields.

resonance fields, and this comparison is shown in Fig. 4. The mass of the sample (∼0.1 mg) is too small to calculate the correct magnetization values, and thus we used the raw magnetization data. As obviously shown in Fig. 4, the ESR signal intensities are proportional to the magnetization values at the resonance fields above 135 K. However, I_D at 130 K significantly deviates from trends observed at higher

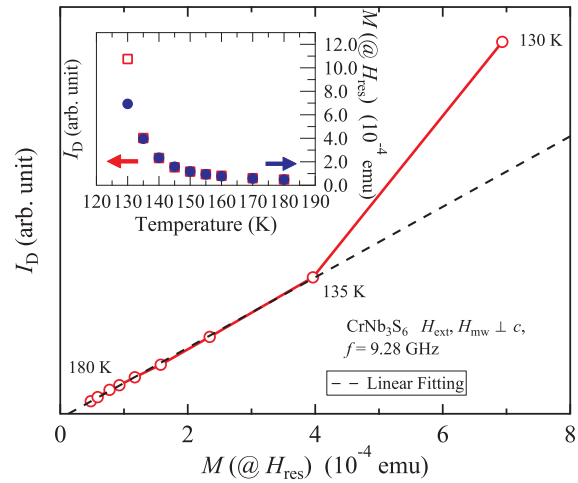

FIG. 4. Comparison of the signal intensities I_D and the magnetization values M at $H_{\text{ext}} = H_{\text{res}}$ for $H_{\text{ext}} \perp c$. The broken line is the result of the linear fitting except the data at 130 K. The inset indicates the simultaneous plots of the temperature dependences of I_D (open red squares) and M (solid blue circles) at $H_{\text{ext}} = H_{\text{res}}$.

temperatures, and this change in behavior is clearly shown in the inset of Fig. 4. This result indicates that the FM state with the DM interactions is developed, although the temperature is above the transition temperature $T_c = 127$ K. Previous ac magnetic susceptibility measurements show similar results. A large third harmonic component $M'_{3\omega}$ and a large out-of-phase component of $M'_{1\omega}$ were observed below about 135 K [25].

In addition, the shift of the resonance field H_{res} changes drastically below 140 K as mentioned in the previous section. This is probably caused by the ferromagnetic resonance (FMR) including the demagnetization factors given by the following equation for the magnetic field applied parallel to the plane:

$$\omega_0 = \gamma[B_0(B_0 + 4\pi M)]^{1/2}, \quad (3)$$

where ω_0 is the angular frequency ($=2\pi f$), γ ($=g\mu_B/\hbar$) is the magnetogyric ratio, B_0 is the resonance magnetic flux density ($=\mu_0 H_{res}$, $\mu_0 \equiv$ permeability in vacuum), and M is the magnetization (G) which is normalized to meet the observed H_{res} at 130 K. The open squares above 130 K in Fig. 3, which are the calculated FMR fields, agree well with experimental results. This FMR with the demagnetization factor below 180 K is probably caused by strong FM interactions in the *ab* plane [23,24]. Because of the large intralayer FM interactions, magnetic moments in $CrNb_3S_6$ are aligned only in the *ab* plane above T_c. This idea is supported by the previous magnetic entropy measurement which suggested the FM correlations might be present even at higher temperature than T_c [30].

B. Below the transition temperature ($T < T_c$)

When $T < T_c$, the ESR line shape is deformed from a simple Dysonian curve and the CSL phase is established due to the combined effect of the DM interactions and the interlayer FM coupling. It is difficult to analyze the spectra successfully by fitting them with some resonance functions such as the Lorentzian and the Dysonian functions, because their shapes are too complex. These complex spectra may arise from the high-temperature CSL state of $CrNb_3S_6$. The shapes of ESR spectra at $90 < T < 115$ K are more complicated than those at other temperature ranges. It is hard to analyze the observed ESR spectra and thus identify accurate resonance fields mentioned above, but we observed some deformed signals at $T = 3.5$ K. The dip near 1900 Oe may correspond to the theoretical ESR signal reported by Kishine and Ovchinnikov [26]. In their paper, the resonance branches originated from CSL magnetic structure are almost field independent, and rapidly decrease near the saturation magnetic field. The ESR signal observed when $H < 1$ kOe is not predicted theoretically and its origin is not clear at the moment.

IV. DISCUSSION

The ESR signal above T_c is explained by a single Dysonian function. Below T_c, several ESR signals were observed, and interesting anomalies were observed. As shown in Fig. 1, the spiked anomalies were observed below 105 K. Figure 5(a) shows the ESR signals at 3.5 K, and the spiked anomalies were clearly seen below 1000 Oe. In order to identify the

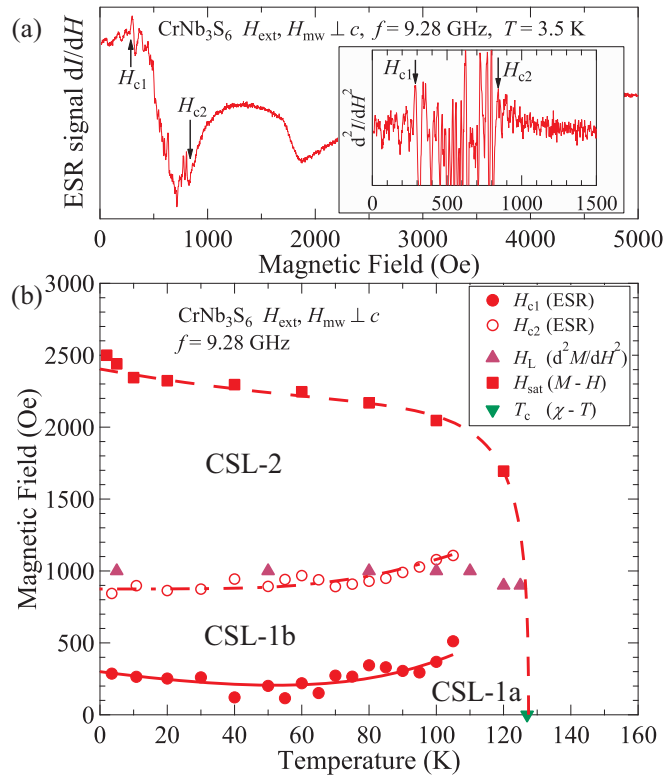

FIG. 5. (a) ESR signal at $T = 3.5$ K for $H_{ext} \perp c$ and $H_{mw} \perp c$ (Fig. 2). The H_{c1} and H_{c2} indicate the appearing and disappearing fields of the spiked anomalies in the ESR signal, respectively. The inset shows the expanded view of d^2I/dH^2. At $H_{c1} < H < H_{c2}$, intense peaks were observed. (b) Magnetic field vs temperature phase diagram of $CrNb_3S_6$. The red solid and open circles indicate the H_{c1} and H_{c2}, respectively, and the solid red squares represent the saturation magnetic fields derived from the magnetization curves. The purple triangles are plotted from the d^2M/dH^2 curve in the magnetization measurements [25], and the green inverted triangle is plotted from the temperature dependence of magnetic susceptibility [25]. The red dashed, dot-dashed, and solid lines are guides to the eyes.

field region where the anomalies exist, we plotted the second field derivative of the signal intensity (d^2I/dH^2) as shown in the inset of Fig. 5(a). These spiked anomalies are not caused by the measurement system because they are much larger than the white noise observed above 1000 Oe [the inset of Fig. 5(a)] and they have not been observed without the sample. Furthermore, these spiked anomalies are not random noise because their shapes are relatively insensitive to changes of the amplitude and frequency of the modulation magnetic field (0.5–8 G and 12.5–100 kHz, respectively), the microwave power (0.2–20 mW) and the time constant (81–655 msec), and by the thermal cycles (three times from room temperature to 3.5 K). Therefore, the spiked anomalies must be intrinsic signals in the CSL phase of $CrNb_3S_6$.

We determine the appearing and disappearing fields of the spiked anomalies (H_{c1} and H_{c2}) by the d^2I/dH^2 for all the measured temperatures, and plot them in the magnetic field vs temperature phase diagram [the red solid and open circles in Fig. 5(b)]. It should be noted that these boundaries are

not thermodynamic phase transitions but merely crossovers observed by dynamical ESR responses. Therefore, the foundations of Dzyaloshinskii's theory [10] are not applicable in this discussion. In this figure, the saturation magnetization fields H_{sat} derived from the magnetization curves and the transition temperature to a long-range helical ordered state at zero field are also plotted as the red solid squares and the green inverted triangle, respectively. The solid and open circles traverse the area surrounded by these squares and the inverted triangle, indicating that the H_{c1} and H_{c2} are two boundaries between the CSL-1a and the CSL-1b, and between the CSL-1b and the CSL-2 regions, respectively, in Fig. 5(b). The boundary indicated by open circles agrees with those plotted by the purple triangles in Fig. 5(b) which are determined from the d^2M/dH^2 curve of $CrNb_3S_6$ in the magnetization measurements [25]. The CSL-1 and 2 areas were named from the magnetization measurements. The boundary determined from the disappearing field H_{c2} nearly corresponds to that determined from the d^2M/dH^2 [18], magnetic entropy curve [30], and magnetization [31]. Therefore the spiked anomalies appear in the linear magnetization region of the CSL state, where magnetic soliton density is high enough and the solitons probably do not move easily, in $CrNb_3S_6$. Other evidence for the correlation between the CSL state and spiked anomalies is the angular dependence of the spiked anomalies as shown in Fig. 6(a). The field region of the spiked anomalies shifts to higher field side and widens, when the magnetic field is rotated from the direction perpendicular to the c axis to that parallel to the c axis. When the magnetic field is almost perfectly parallel to the c axis, the spiked anomalies disappear from the window of the measurement magnetic field. The angular dependences of H_{c1} and H_{c2} are shown in Fig. 6(b). The solid lines are the results of fittings with the following expression:

$$H_{ci} = a_i/|\cos\theta| + b_i, \quad i = 1, 2, \tag{4}$$

where a_i is a coefficient, θ is the applied field angle, and b_i is a constant. Both H_{c1} and H_{c2} are well fitted with this equation ($a_1 = 0.432$, $b_1 = 0.055$, $a_2 = 0.910$, and $b_2 = 0.010$), but we do not know the origin of the angular dependence.

Next, we consider the origin of these spiked anomalies. The Walker mode which appears in some ferromagnets is negligible because the wavelength of emitted microwave (∼33 mm at ∼9 GHz) is sufficiently longer than the sample size (⩽1 mm). Furthermore, they do not alter their structure by changing the experimental parameters as written above. Thus, the origin of the spiked anomalies is not clear at present. The magnetic structure in the CSL-1a region in Fig. 5(b) is close to the chiral helimagnetic structure (CHS) and then the density of the ferromagnetic region is quite low and the ferromagnetic domains cannot correlate each other because of the large distance between them [18]. Some reports suggest that the CSL-1b region in our phase diagram also possesses the CHS and the boundary determined by H_{c2} corresponds to the CHS-CSL crossover line. However, the observation of the spiked anomalies only in the CSL-1b region is opposed to this idea of CHS-CSL crossover, because the CHS in the CSL-1a region does not cause such an unusual response. Consequently, we do not have an interpretation of the spiked anomaly region. Finally, we discuss the distance between the magnetic solitons (helical region of the CSL structure) that is larger in the CSL-2 region than in the CSL-1b region. The spiked anomalies only appear in the CSL-1b region because the distance between the magnetic solitons may be appropriate only in this region.

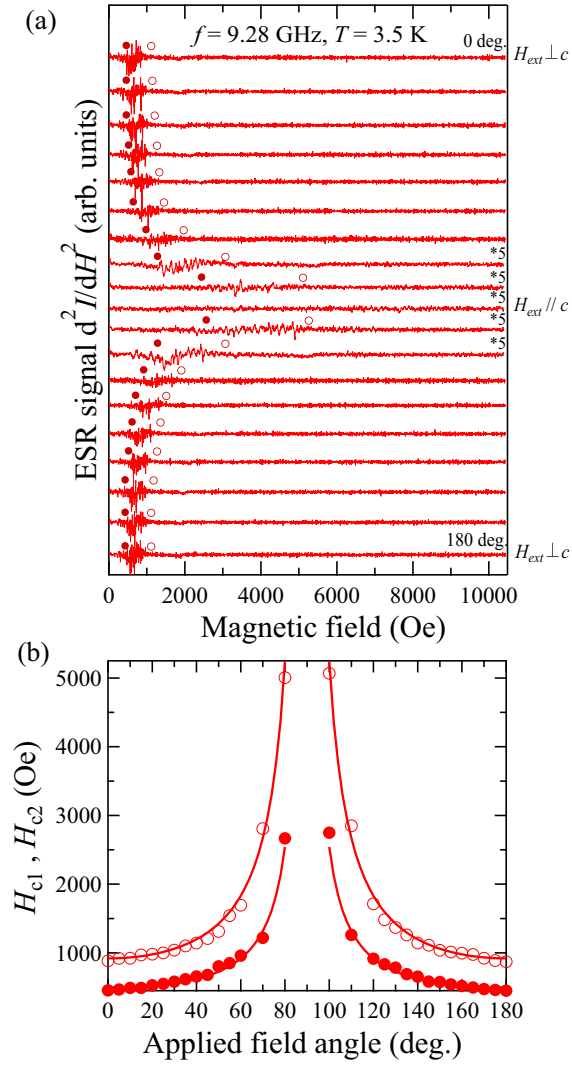

FIG. 6. (a) Angular dependence of the spiked anomalies shown by d^2I/dH^2 to clarify the anomalous field region. The data are displayed every 10° from 0° ($H_{ext} \perp c$) to 180°. The solid and open circles indicate the appearing and disappearing fields of the spiked anomalies (H_{c1} and H_{c2}), respectively. The field region of the spiked anomalies shifts to higher field and widens, when the magnetic field is rotated from the direction perpendicular to the c axis to that parallel to the c axis, and moves to the out of range for the c axis. (b) The angular dependence of H_{c1} and H_{c2}. The data are plotted by the same symbols as in Fig. 6(a). Both solid lines are the results of the fittings with Eq. (4).

V. SUMMARY

In summary, we have performed X-band ESR measurements of a single crystal of $CrNb_3S_6$ in magnetic fields perpendicular to the c axis (helical axis). The observed main ESR signal above T_c is fitted by the single Dysonian function.

In addition, we observed spiked anomalies superposed on unusual ESR signals below 105 K. These spiked anomalies exist in a range of magnetic fields bounded by H_{c1} and H_{c2}, i.e., $H_{c1} < H < H_{c2}$. The resulting magnetic field versus temperature phase diagram identifies the CSL state as having three distinct regions in terms of dynamic responses in the gigahertz regime. Correlations between magnetic solitons in the intermediate region, CSL-1b of Fig. 5, may be the source of the spiked anomalies.

ACKNOWLEDGMENTS

We thank K. Tsuruta at JASRI/SPring-8 for fruitful discussions. This work was partially supported by Grants-in-Aid for Scientific Research (S) Grant No. 25220803, Scientific Research (A) Grant No. 24244059, Scientific Research (A) Grant No. 25246006, Scientific Research (C) Grant No. 26400368, and Scientific Research (B) Grant No. 15H03680 all from MEXT, and by JSPS Core-to-Core Program, A. Advanced Research Network.

[1] I. E. Dzyaloshinskii, Sov. Phys. JETP **5**, 1259 (1957).
[2] T. Moriya, Phys. Rev. **120**, 91 (1960).
[3] I. E. Dzyaloshiskii, Sov. Phys. JETP **19**, 960 (1964).
[4] Y. Ishikawa, K. Tajima, D. Bloch, and M. Roth, Solid State Commun. **19**, 525 (1976).
[5] S. V. Grigoriev, V. A. Dyadkin, D. Menzel, J. Schoenes, Y. O. Chetverikov, A. I. Okorokov, H. Eckerlebe, and S. V. Maleyev, Phys. Rev. B **76**, 224424 (2007).
[6] T. Miyadai, K. Kikuchi, H. Kondo, S. Sakka, M. Arai, and Y. Ishikawa, J. Phys. Soc. Jpn. **52**, 1394 (1983).
[7] S. Mühlbauer, B. Binz, F. Jonietz, C. Pfleiderer, A. Rosch, A. Neubauer, R. Georgii, and P. Böni, Science **323**, 915 (2009).
[8] X. Z. Yu, Y. Onose, N. Kanazawa, J. H. Park, J. H. Han, Y. Matsui, N. Nagaosa, and Y. Tokura, Nature (London) **465**, 901 (2010).
[9] S. Seki, X. Z. Yu, S. Ishiwata, and Y. Tokura, Science **336**, 198 (2012).
[10] I. E. Dzyaloshinskii, Sov. Phys. JETP **20**, 665 (1965).
[11] J.-i. Kishine, K. Inoue, and Y. Yoshida, Prog. Theor. Phys. Suppl. **159**, 82 (2005).
[12] I. G. Bostrem, J.-i. Kishine, and A. S. Ovchinnikov, Phys. Rev. B **77**, 132405 (2008).
[13] I. G. Bostrem, J.-i. Kishine, and A. S. Ovchinnikov, Phys. Rev. B **78**, 064425 (2008).
[14] Y. Togawa, T. Koyama, K. Takayanagi, S. Mori, Y. Kousaka, J. Akimitsu, S. Nishihara, K. Inoue, A. S. Ovchinnikov, and J.-i. Kishine, Phys. Rev. Lett. **108**, 107202 (2012).
[15] Y. Togawa, Y. Kousaka, S. Nishihara, K. Inoue, J. Akimitsu, A. S. Ovchinnikov, and J.-i. Kishine, Phys. Rev. Lett. **111**, 197204 (2013).
[16] Y. Togawa, T. Koyama, Y. Nishimori, Y. Matsumoto, S. McVitie, D. McGrouther, R. L. Stamps, Y. Kousaka, J. Akimitsu, S. Nishihara, K. Inoue, I. G. Bostrem, V. E. Sinitsyn, A. S. Ovchinnikov, and J.-i. Kishine, Phys. Rev. B **92**, 220412 (2015).
[17] J.-i. Kishine and A. S. Ovchinnikov, Solid State Phys. **66**, 1 (2015).
[18] K. Tsuruta, M. Mito, Y. Kousaka, J. Akimitsu, J.-i. Kishine, Y. Togawa, H. Ohsumi, and K. Inoue, J. Phys. Soc. Jpn. **85**, 013707 (2016).
[19] Y. Togawa, Y. Kousaka, K. Inoue, and J.-i. Kishine, J. Phys. Soc. Jpn. **85**, 112001 (2016).
[20] F. Hulliger and E. Pobitschka, J. Solid State Chem. **1**, 117 (1970).
[21] Y. Kousaka, Y. Nakao, J.-i. Kishine, M. Akita, K. Inoue, and J. Akimitsu, Nucl. Instrum. Methods Phys. Res., Sect. A **600**, 250 (2009).
[22] L. M. Volkova and D. V. Marinin, J. Appl. Phys. **116**, 133901 (2014).
[23] D. Yoshizawa, J.-i. Kishine, Y. Kousaka, Y. Togawa, M. Mito, J. Akimitsu, K. Inoue, and M. Hagiwara, Phys. Proc. **75**, 926 (2015).
[24] M. Shinozaki, S. Hoshino, Y. Masaki, J.-i. Kishine, and Y. Kato, J. Phys. Soc. Jpn. **85**, 074710 (2016).
[25] K. Tsuruta, M. Mito, H. Deguchi, J.-i. Kishine, Y. Kousaka, J. Akimitsu, and K. Inoue, Phys. Rev. B **93**, 104402 (2016).
[26] J.-i. Kishine and A. S. Ovchinnikov, Phys. Rev. B **79**, 220405 (2009).
[27] F. J. T. Goncalves, T. Sogo, Y. Shimamoto, Y. Kousaka, J. Akimitsu, S. Nishihara, K. Inoue, D. Yoshizawa, M. Hagiwara, M. Mito, R. L. Stamps, I. G. Bostrem, V. E. Sinitsyn, A. S. Ovchinnikov, J. Kishine, and Y. Togawa, Phys. Rev. B **95**, 104415 (2017).
[28] E. Dengler, J. Deisenhofer, H.-A. Krug von Nidda, S. Khim, J. S. Kim, K. H. Kim, F. Casper, C. Felser, and A. Loidl, Phys. Rev. B **81**, 024406 (2010).
[29] S. E. Barnes, Adv. Phys. **30**, 801 (1981).
[30] E. M. Clements, R. Das, L. Li, P. J. Lampen-Kelley, M.-H. Phan, V. Keppens, D. Mandrus, and H. Srikanth, Sci. Rep. **7**, 6545 (2017).
[31] N. J. Ghimire, M. A. McGuire, D. S. Parker, B. Sipos, S. Tang, J.-Q. Yan, B. C. Sales, and D. Mandrus, Phys. Rev. B **87**, 104403 (2013).